JOURNAL OF GUIDANCE, CONTROL, AND DYNAMICS
Vol. 36, No. 5, September–October 2013

Spacecraft Attitude Stabilization Using Nonlinear Delayed Multiactuator Control and Inverse Dynamics

Morad Nazari* and Eric A. Butcher†
New Mexico State University, Las Cruces, New Mexico 88003
and
Hanspeter Schaub‡
University of Colorado, Boulder, Colorado 80309-0431

DOI: 10.2514/1.58249

The dynamics of a rigid spacecraft with nonlinear delayed multiactuator feedback control are studied in this paper. It is assumed that the time delay occurs in one of the actuators, whereas the other actuator has a negligible time delay. Therefore, a nonlinear feedback controller using both delayed and nondelayed states is sought for the controlled system to have the desired linear delayed closed-loop dynamics using an inverse dynamics approach. The closed-loop stability is shown to be approximated by a second-order linear delay differential equation for the modified Rodriguez parameter attitude coordinates for which the Hsu–Bhatt–Vyshnegradskii stability chart can be used to choose the control gains that result in a stable closed-loop response. An analytical derivation of the boundaries of this chart for the case of no derivative feedback control is shown, whereas a numerical method is used to obtain the stability chart for the general case. Then, to achieve a specified performance, the criteria for a critically damped closed-loop response are studied. Further, an integral feedback control is also implemented, which is capable of eliminating the steady-state attitude error caused by any unmodeled external torque.

Nomenclature

$\mathcal{A}$	=	infinitesimal generator of the solution operator
D	=	Chebyshev spectral differentiation matrix
J	=	inertia matrix in principal coordinates
K	=	proportional control gain
K_i	=	integral control gain
L	=	true external torque
L^*	=	modeled external torque
P	=	derivative control gain
R	=	delay control gain
u	=	feedback control law
V	=	Lyapunov candidate
x, y	=	assembled state-space vectors
z	=	assembled state-space vector for the transformed delayed equations
ΔL	=	unmodeled external torque
σ	=	modified Rodriguez parameter set
τ	=	time delay, s
ω	=	angular velocity vector, rad/s

I. Introduction

THE NONLINEAR control of spacecraft attitude dynamics with time-delayed feedback is considered in this study. Time delays arise due to communication delays, including delays in the measurement, or processing delays, including delays that occur in the actuators. The latter case is studied in this paper, and in particular, the case of multiactuator control with nonnegligible time delays in one of the actuators is addressed.

The attitude modeling problem depends on the choice of attitude parameters (coordinates) to represent the orientation of a rigid body relative to an inertial frame. There are several different attitude parameterizations, which can be used to obtain the governing spacecraft equations. Minimal three-coordinate sets include Euler angles, classical Rodriguez parameters, and modified Rodriguez parameters (MRPs). MRPs are used for the attitude parameterization in this paper.

The simultaneous use of multiple types of actuators, including maneuvers involving the simultaneous use of reaction wheels (RWs) or control moment gyros (CMGs) and reaction control thrusters (RCTs), has a variety of applications, including developing tracking control laws [1,2], achieving RW or CMG desaturation, and using the null motion to reorient CMG clusters to avoid singularities [3]. For instance, three types of multiactuator controllers were used by Hall et al. [1] to globally asymptotically stabilize the closed-loop dynamics of spacecraft. Two of the controllers use thrusters for bang-bang control and RWs to provide the necessary corrections, whereas the third one uses linear feedback for the RWs and nonlinear feedback for the thrusters. A method was developed by Paielli and Bach [4] for controlling the spacecraft attitude by implementing a rigorous nonlinear control that results in linear closed-loop dynamics and thus retains almost global nonlinear stability. This inverse dynamics approach contrasts sharply from developing linearized closed-loop dynamics, which are only valid in a local neighborhood, and is a general technique common in other disciplines such as robotics. Although the controller in [4] used Euler parameters (see also [3]), Schaub et al. [5] proposed an adaptive attitude control law in conjunction with an inverse dynamics approach using MRPs to track the desired linear performance in the presence of unknown external disturbance without requiring prior information about the inertia. It was shown (see also [3]) that the MRP feedback control necessary to obtain linear closed-loop dynamics is only slightly more complicated than the corresponding control using Euler parameters but results in globally asymptotically stable motion.

The stability analysis of time-delayed systems or delay differential equations (DDEs) is important in many fields. Two general strategies for obtaining stability conditions include the frequency-based approach, which determines spectral stability conditions for linear time-invariant DDEs, and the Lyapunov-based time domain approach,

Presented as Paper AAS 2012-237 at the 22nd AAS/AIAA Space Flight Mechanics Meeting, Charleston, South Carolina, 29 January 2012–2 February 2012; received 12 March 2012; revision received 10 November 2012; accepted for publication 9 January 2013; published online 24 July 2013.

*Ph.D. Student, Mechanical and Aerospace Engineering Department. Student Member AIAA.

†Associate Professor, Dwight and Aubrey Chapman Endowed Professor, Mechanical and Aerospace Engineering Department. Member AIAA.

‡Associate Professor, H. Joseph Smead Fellow, Aerospace Engineering Sciences Department. Associate Fellow AIAA.

which can be applied to a wider range of DDEs, including those with nonlinearities and time-varying coefficients. In the latter class, the Lyapunov–Krasovskii (L–K) functional and Lyapunov–Razumikhin function are two major methods used to obtain stability conditions in the framework of Lyapunov's direct method. Recently, new constructions of the L–K functionals have been developed for the analysis of stability and region of attraction for nonlinear systems with time delays. A modified L–K functional was developed, in particular, by Chunodkar and Akella [6] to obtain the region of attraction for spacecraft attitude stabilization with unknown but bounded delay in the linear feedback control. Exponential stability is obtained for all values of the time delay within the appropriate bounds. A velocity-free controller was designed by Ailon et al. [7] for delayed attitude regulation of a rigid spacecraft. Sufficient conditions for exponential stability of the controlled response were established.

In this paper, the MRP-based inverse dynamics control used in [3,5] is extended to address the multiactuator delayed feedback attitude control of a rigid spacecraft in which one actuator is nondelayed, whereas the other one has a nonnegligible time delay. This strategy could possibly be extended to desaturation maneuvers that involve the simultaneous use of two different actuators (e.g., RWs and RCTs), although the current form does not take internal momentum management into account because the design is based on rigid-body rotational dynamics. We also consider the strategy of delay stabilization by intentionally increasing either the gain of the delayed actuator or the time delay itself in order to stabilize an otherwise unstable closed-loop dynamics without delay. The closed-loop stability is shown to be approximated by a second-order linear DDE for the MRP attitude coordinates for which the Hsu–Bhatt–Vyshnegradskii stability chart can be used to choose the control gains that result in a stable closed-loop response. An analytical derivation of the boundaries of this chart for the case of no derivative feedback control is shown, whereas a numerical method is used to obtain the stability chart for the general case. Then, to achieve a specified performance, the criteria for a critically damped closed-loop response are studied. Further, an integral feedback control is also implemented, which is capable of eliminating the steady-state attitude error caused by any unmodeled torque.

II. Attitude Dynamics Model

In terms of the principal rotation elements, the MRP attitude parameterization $\sigma \in \mathbb{R}^3$ is defined as

$$\sigma = \tan\frac{\Phi}{4}\hat{e} \tag{1}$$

where Φ is the principal rotation angle about the principal rotation axis $\hat{e}$. When used with the constraint that $\|\sigma\| \leq 1$ by switching to the shadow set [3] when $\Phi = 180$ deg, the MRPs are a singularity-free unique global attitude description.

Euler's equations for controlled rigid-body rotation can be written as

$$J\dot{\omega} + \tilde{\omega}J\omega = L^* + \Delta L + u(t) \tag{2}$$

where $\omega(t) \in \mathbb{R}^3$ represents the angular velocity of the body frame with respect to the inertial frame, and $J \in \mathbb{R}^{3\times3}$ is the inertia matrix calculated about the center of mass. L^* is a modeled external torque, ΔL represents an unmodeled torque, and $u(t)$ is the applied control torque. Note that $\tilde{(\cdot)}: \mathbb{R}^3 \to \mathrm{so}(3)$ is the skew-symmetric mapping given by

$$\tilde{\Psi} = \begin{bmatrix} 0 & -\Psi_3 & \Psi_2 \\ \Psi_3 & 0 & -\Psi_1 \\ -\Psi_2 & \Psi_1 & 0 \end{bmatrix} \tag{3}$$

where the space of 3×3 real skew-symmetric matrices is denoted by so(3), the Lie algebra of the Lie group SO(3). Equation (2) along with the kinematic differential equations in terms of the MRPs,

$$\dot{\sigma} = \frac{1}{4}B(\sigma)\omega, \qquad B(\sigma) = [(1-\sigma^T\sigma)I_3 + 2\tilde{\sigma} + 2\sigma\sigma^T] \tag{4}$$

specify the governing dynamical equations of the system, where I_3 is the three-dimensional identity matrix. The current state of the system at time t is given by $[\sigma^T(t)\omega^T(t)]^T$, whereas the delayed state is $[\sigma^T(t-\tau)\omega^T(t-\tau)]^T$, where τ is the time delay.

III. Inverse Dynamics Approach for Feedback Control Law

Figure 1 shows the block diagram of the system with a time delay in one of the actuators (as opposed to the case in which a time delay exists in the measurements [8]), in which the output can be any of the state vectors of the system or a combination of them. By introducing the system with two actuators as shown in the block diagram in Fig. 1, in which the nondelayed actuator 1 with gains P and K feeds back the current state $[\sigma(t), \omega(t)]$, whereas the delayed actuator 2 with gain R feeds back the delayed attitude $\sigma(t-\tau)$ only, we consider the problem of multiactuator control, which has applications in desaturation maneuvers, for instance. Thus, for linear feedback control (which is not used in this paper), the control force for actuator 1 would be $u_1(t) = -P\omega(t) - K\sigma(t)$, whereas that for the delayed actuator 2 would be $u_2(t) = -R\sigma(t-\tau)$. A related problem is the concept of delay stabilization by intentionally increasing either the gain of the delayed actuator or the time delay itself in order to stabilize an otherwise unstable closed-loop dynamics.

There are different approaches for controlling the attitude dynamics of a rigid body. One method is to assume a linear control law, which results in a nonlinear model for the closed-loop dynamics of the system [7,8]. Another method is to assume a nonlinear control law, which results in a linear model for the closed-loop dynamics of the system [3]. This second approach will be used here. In particular, an inverse dynamics approach common in robotics open-loop path-planning problems is used here, in which the desired closed-loop response is approximated by a set of second-order delay differential equations. This approach (without time delay) has been used in the attitude control problem using both quaternions [4] and MRPs [3].

Based on the desired linear closed-loop dynamics for the nondelayed case of MRP-based attitude control [3], for the delayed system, we choose the desired closed-loop system to be the linear system of second-order DDEs given by

$$\ddot{\sigma}(t) + P\dot{\sigma}(t) + K\sigma(t) = R\sigma(t-\tau) \tag{5}$$

In the general case, P, K, and R could be full 3×3 matrices. However, in this paper, we choose P, K, and R to be scalars such that Eq. (5) decouples into three identical scalar second-order DDEs. As is explained in the preceding section, τ is the time delay in actuator 2 of Fig. 1. The justification for Eq. (5) is as follows. First, as mentioned previously, this is similar to the inverse dynamics strategies used in [3–5], which used the same closed-loop dynamics as Eq. (5) except with $R = 0$ and in which good attitude tracking performances were obtained for globally or almost globally asymptotically stable behavior. Next, because one actuator has an unavoidable time delay, the resulting closed-loop system will be a DDE. Here, we choose the DDE to be linear. Further, no system properties such as inertia are included, a property beneficial in adaptive control strategies. Finally, since the three components of Eq. (5) decouple, the stability properties of each of the resulting scalar DDEs can be obtained, analytically or numerically, in terms of P, K, R, and τ. Especially for

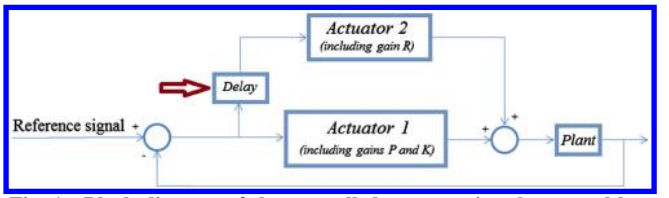

Fig. 1 Block diagram of the controlled system using the control law given in Eq. (31) with the time delay in one of the actuators.

the case in which $P = 0$, the analytical stability conditions are well known [9,10].

We now present the main theoretical result that will enable a nonlinear control law to be designed such that the resulting closed-loop system is approximated to order τ by Eq. (5).

Lemma: The body angular acceleration vector corresponding to Eq. (5) can be simplified to

$$\dot{\omega} = -P\omega - \left[\omega\omega^T + \left(\frac{4K}{1+\|\sigma\|^2} - \frac{\|\omega\|^2}{2}\right)I_3\right]\sigma + 4B^{-1}(\sigma)R\sigma(t-\tau) \tag{6}$$

Proof: Differentiating both sides of the kinematic differential equations given in Eq. (4) and substituting the result back into Eq. (5) yields

$$\ddot{\sigma} + P\dot{\sigma} + K\sigma = \frac{1}{4}B(\sigma)[\dot{\omega} + P\omega + B^{-1}(\sigma)(\dot{B}(\sigma)\omega + 4K\sigma)] = R\sigma(t-\tau) \tag{7}$$

Because $B^{-1}(\sigma)$ always exists for $\|\sigma\| < 1$, Eq. (7) becomes [3]

$$\dot{\omega} + P\omega + B^{-1}(\sigma)(\dot{B}(\sigma)\omega + 4K\sigma) = 4B^{-1}(\sigma)R\sigma(t-\tau) \tag{8}$$

Taking the time derivative of matrix $B(\sigma)$ in Eq. (4),

$$\dot{B}(\sigma) = (-\dot{\sigma}^T\sigma - \sigma^T\dot{\sigma})I_3 + 2\dot{\tilde{\sigma}} + 2\dot{\sigma}\sigma^T + 2\sigma\dot{\sigma}^T \tag{9}$$

$$\dot{\sigma}^T = \frac{1}{4}\omega^T[(1-\|\sigma\|^2)I_3 - 2\tilde{\sigma} + 2\sigma\sigma^T] \tag{10}$$

On the other hand,

$$\tilde{\sigma}^2 = \sigma\sigma^T - \|\sigma\|^2 I_3 = \sigma\sigma^T - \sigma^T\sigma I_3 \tag{11}$$

Taking the time derivative of both sides of Eq. (11), we obtain

$$\tilde{\sigma}\dot{\tilde{\sigma}} + \dot{\tilde{\sigma}}\tilde{\sigma} = \dot{\sigma}\sigma^T + \sigma\dot{\sigma}^T - (\dot{\sigma}^T\sigma + \sigma^T\dot{\sigma})I_3 = E \tag{12}$$

Now, defining

$$F \triangleq \tilde{\sigma}\dot{\tilde{\sigma}}, \qquad F^T \triangleq \dot{\tilde{\sigma}}\tilde{\sigma} \tag{13}$$

Equation (12) can be written as

$$F + F^T = E \tag{14}$$

Furthermore,

$$F - F^T = \begin{pmatrix} 0 & \sigma_2\dot{\sigma}_1 - \sigma_1\dot{\sigma}_2 & \dot{\sigma}_1\sigma_3 - \sigma_1\dot{\sigma}_3 \\ \dot{\sigma}_2\sigma_1 - \sigma_2\dot{\sigma}_1 & 0 & \dot{\sigma}_2\sigma_3 - \dot{\sigma}_3\sigma_2 \\ \dot{\sigma}_3\sigma_1 - \sigma_3\dot{\sigma}_1 & \dot{\sigma}_3\sigma_2 - \sigma_3\dot{\sigma}_2 & 0 \end{pmatrix} = \dot{\sigma}\sigma^T - \sigma\dot{\sigma}^T = G \tag{15}$$

Equations (14) and (15) can be solved for F and F^T as

$$\tilde{\sigma}\dot{\tilde{\sigma}} = F = \frac{1}{2}(E+G) = \dot{\sigma}\sigma^T - \frac{1}{2}(\dot{\sigma}^T\sigma + \sigma^T\dot{\sigma})I_3,$$
$$\dot{\tilde{\sigma}}\tilde{\sigma} = F^T = \sigma\dot{\sigma}^T - \frac{1}{2}(\sigma^T\dot{\sigma} + \dot{\sigma}^T\sigma)I_3 \tag{16}$$

Also, note that

$$B^T(\sigma) = (1+\|\sigma\|^2)^2 B^{-1}(\sigma) \tag{17}$$

As shown in Eq. (9), $\dot{B}(\sigma)\omega$ has a term $\dot{\tilde{\sigma}}\omega$. But, Eq. (10) implies that

$$\omega = 4B^{-1}(\sigma)\dot{\sigma} = \frac{4B^T(\sigma)}{(1+\|\sigma\|^2)^2}\dot{\sigma} \tag{18}$$

Hence,

$$\dot{\tilde{\sigma}}\omega = \dot{\tilde{\sigma}}\frac{4B^T(\sigma)}{(1+\|\sigma\|^2)^2}\dot{\sigma} = \frac{4}{(1+\|\sigma\|^2)^2}[(1-\|\sigma\|^2)\dot{\tilde{\sigma}}\dot{\sigma} - 2\dot{\tilde{\sigma}}\tilde{\sigma}\dot{\sigma} + 2\dot{\tilde{\sigma}}\sigma\sigma^T\dot{\sigma}] \tag{19}$$

where the first term inside the brackets is zero. According to Eq. (11), the last term inside the brackets can be expressed as

$$2\dot{\tilde{\sigma}}(\sigma\sigma^T)\dot{\sigma} = 2\dot{\tilde{\sigma}}(\tilde{\sigma}^2 + \sigma^T\sigma I_3)\dot{\sigma} = 2(\dot{\tilde{\sigma}}\sigma)(\tilde{\sigma}\dot{\sigma}) + 2(\sigma^T\sigma)(\dot{\tilde{\sigma}}\dot{\sigma}) = 2(\dot{\tilde{\sigma}}\tilde{\sigma})(\tilde{\sigma}\dot{\sigma}) \tag{20}$$

After some manipulation, Eq. (19) can therefore be written as

$$\dot{\tilde{\sigma}}\omega = \frac{4}{(1+\|\sigma\|^2)^2}(-2\dot{\tilde{\sigma}}\tilde{\sigma}\dot{\sigma} + 2\dot{\tilde{\sigma}}\tilde{\sigma}\tilde{\sigma}\dot{\sigma}) = \frac{8\dot{\tilde{\sigma}}\tilde{\sigma}}{(1+\|\sigma\|^2)^2}(-I_3 + \tilde{\sigma})\dot{\sigma} = -\frac{2\dot{\tilde{\sigma}}\tilde{\sigma}}{1+\|\sigma\|^2}(I_3 + \tilde{\sigma})\omega \tag{21}$$

where Eqs. (4) and (11) are used to obtain the simplified form given in Eq. (21) for $\dot{\tilde{\sigma}}\omega$.

However, by substituting for $\dot{\tilde{\sigma}}\tilde{\sigma}$ from Eq. (16) into Eq. (21), we obtain

$$\begin{aligned}
\dot{\tilde{\sigma}}\omega &= -\frac{2}{1+\|\sigma\|^2}\left[\sigma\dot{\sigma}^T - \frac{1}{2}(\sigma^T\dot{\sigma} + \dot{\sigma}^T\sigma)I_3\right](I_3 + \tilde{\sigma})\omega \\
&= \frac{2}{1+\|\sigma\|^2}(-\sigma\dot{\sigma}^T + \sigma^T\dot{\sigma}I_3)(I_3 + \tilde{\sigma})\omega \\
&= \frac{2}{1+\|\sigma\|^2}\left\{-\frac{\sigma\omega^T}{4}[(1-\|\sigma\|^2)I_3 - 2\tilde{\sigma} + 2\sigma\sigma^T] + \frac{\sigma^T}{4}[(1-\|\sigma\|^2)I_3 + 2\tilde{\sigma} + 2\sigma\sigma^T]\omega I_3\right\}(I_3 + \tilde{\sigma})\omega \\
&= \frac{1}{2(1+\|\sigma\|^2)}\{-(1-\|\sigma\|^2)\sigma\omega^T + 2\sigma\omega^T\tilde{\sigma} - 2\sigma\omega^T\sigma\sigma^T \\
&\quad + [(1-\|\sigma\|^2)\sigma^T + 2\sigma^T\tilde{\sigma} + 2\sigma^T\sigma\sigma^T]\omega I_3\}(I_3 + \tilde{\sigma})\omega \\
&= \frac{1}{2(1+\|\sigma\|^2)}\{-(1-\|\sigma\|^2)\sigma\|\omega\|^2 - 2\sigma\omega^T\tilde{\omega}\sigma - 2(\sigma^T\omega)^2\sigma \\
&\quad + (1-\|\sigma\|^2)(\sigma^T\omega)\omega + 2\|\sigma\|^2(\sigma^T\omega)\omega \\
&\quad + (1-\|\sigma\|^2)\sigma\omega^T\tilde{\omega}\sigma + 2\sigma\omega^T(\sigma\sigma^T - \|\sigma\|^2 I_3)\omega \\
&\quad - 2\sigma\omega^T\sigma\sigma^T\tilde{\sigma}\tilde{\omega} - (1-\|\sigma\|^2)(\sigma^T\omega)(\tilde{\omega}\sigma) - 2\|\sigma\|^2(\sigma^T\omega)\tilde{\omega}\sigma\} \\
&= \frac{1}{2(1+\|\sigma\|^2)}\{(\|\sigma\|^2 - 1)\|\omega\|^2\sigma + (1+\|\sigma\|^2)(\sigma^T\omega)\omega \\
&\quad - 2(\|\sigma\|^2\|\omega\|^2)\sigma - (1+\|\sigma\|^2)(\sigma^T\omega)\tilde{\omega}\sigma\}
\end{aligned} \tag{22}$$

Other terms in Eq. (9) can be simplified as

$$\dot{\sigma}^T\sigma = \sigma^T\dot{\sigma} = \frac{1}{4}\sigma^T B(\sigma)\omega = \frac{1}{4}(1+\|\sigma\|^2)(\sigma^T\omega) \tag{23}$$

$$2\dot{\sigma}(\sigma^T\omega) = \frac{1}{2}[(1-\|\sigma\|^2)I_3 + 2\tilde{\sigma} + 2\sigma\sigma^T](\sigma^T\omega)\omega = \frac{1}{2}(1-\|\sigma\|^2)(\sigma^T\omega)\omega - (\sigma^T\omega)\tilde{\omega}\sigma + (\sigma^T\omega)^2\sigma \tag{24}$$

and

$$2\sigma\dot{\sigma}^T\omega = \frac{1}{2}\sigma\omega^T[(1-\|\sigma\|^2)I_3 - 2\tilde{\sigma} + 2\sigma\sigma^T]\omega$$
$$= \frac{1}{2}(1-\|\sigma\|^2)\|\omega\|^2\sigma + \sigma\omega^T\tilde{\omega}\sigma + (\sigma^T\omega)^2\sigma \quad (25)$$

Substituting Eqs. (22–25) into Eq. (9) yields

$$\dot{B}(\sigma)\omega = -2(\sigma^T\omega)\tilde{\omega}\sigma + 2(\sigma^T\omega)^2\sigma - \frac{1}{2}(1+\|\sigma\|^2)\|\omega\|^2\sigma + (1-\|\sigma\|^2)(\sigma^T\omega)\omega \quad (26)$$

and substituting Eq. (26) into Eq. (8) yields

$$\dot{\omega} = -P\omega - B^{-1}(\sigma)(\dot{B}(\sigma)\omega + 4K\sigma) + 4B^{-1}(\sigma)R\sigma(t-\tau)$$
$$= -P\omega - \frac{B^T(\sigma)}{(1+\|\sigma\|^2)^2}\left[-2(\sigma^T\omega)\tilde{\omega}\sigma + 2(\sigma^T\omega)^2\sigma - \frac{1}{2}(1+\|\sigma\|^2)\|\omega\|^2\sigma + (1-\|\sigma\|^2)(\sigma^T\omega)\omega + 4K\sigma\right] + 4B^{-1}(\sigma)R\sigma(t-\tau)$$
$$= -P\omega - \frac{1}{(1+\|\sigma\|^2)^2}[(1-\|\sigma\|^2)I_3 - 2\tilde{\sigma} + 2\sigma\sigma^T] \times \left[-2(\sigma^T\omega)\tilde{\omega}\sigma + 2(\sigma^T\omega)^2\sigma - \frac{1}{2}(1+\|\sigma\|^2)\|\omega\|^2\sigma + (1-\|\sigma\|^2)(\sigma^T\omega)\omega + 4K\sigma\right] + 4B^{-1}(\sigma)R\sigma(t-\tau)$$
$$- \frac{1}{2}(1+\|\sigma\|^2)(1-\|\sigma\|^2)\|\omega\|^2\sigma + (1-\|\sigma\|^2)^2(\sigma^T\omega)\omega + 4K(1-\|\sigma\|^2)\sigma + 4(\sigma^T\omega)\tilde{\sigma}\,\tilde{\omega}\,\sigma - 2(1-\|\sigma\|^2)(\sigma^T\omega)\tilde{\sigma}\omega + 4(\sigma^T\omega)^2\|\sigma\|^2\sigma - (1+\|\sigma\|^2)\|\omega\|^2\|\sigma\|^2\sigma + 2(1-\|\sigma\|^2)(\sigma^T\omega)^2\sigma + 8K\|\sigma\|^2\sigma] + 4B^{-1}(\sigma)R\sigma(t-\tau) \quad (27)$$

The term $4(\sigma^T\omega)\tilde{\sigma}\,\tilde{\omega}\,\sigma$ in Eq. (27) is expressed as

$$-4(\sigma^T\omega)\tilde{\sigma}^2\omega = -4(\sigma^T\omega)(\sigma\sigma^T - \sigma^T\sigma I_3)\omega$$
$$= -4(\sigma^T\omega)^2\sigma + 4(\sigma^T\omega)\|\sigma\|^2\omega \quad (28)$$

Finally, substituting Eq. (28) into Eq. (27) yields

$$\dot{\omega}(t) = -P\omega - \frac{1}{(1+\|\sigma\|^2)^2}\times\left[(\sigma^T\omega)^2\sigma(2-2\|\sigma\|^2+2 - 2\|\sigma\|^2-4+4\|\sigma\|^2) + (\sigma^T\omega)\omega(1-2\|\sigma\|^2+\|\sigma\|^4+4\|\sigma\|^2) + \|\omega\|^2\sigma\left(-\frac{1}{2}+\frac{\|\sigma\|^4}{2}-\|\sigma\|^2-\|\sigma\|^4\right) + K\sigma(4-4\|\sigma\|^2+8\|\sigma\|^2)\right] + 4B^{-1}(\sigma)R\sigma(t-\tau)$$
$$= -P\omega - \frac{1}{(1+\|\sigma\|^2)^2}\left[\omega(\omega^T\sigma)(1+\|\sigma\|^2)^2 - \frac{1}{2}(1+\|\sigma\|^2)^2\|\omega\|^2\sigma + 4K(1+\|\sigma\|^2)\sigma\right] + 4B^{-1}(\sigma)R\sigma(t-\tau)$$
$$= -P\omega(t) - \left[\omega(t)\omega^T(t) + \left(\frac{4K}{1+\|\sigma(t)\|^2} - \frac{\|\omega(t)\|^2}{2}\right)I_3\right]\sigma(t) + 4\frac{B^T(\sigma(t))}{[1+\|\sigma(t)\|^2]^2}R\sigma(t-\tau) \quad (29)$$

□

Thus, by substituting Eq. (29) into Eq. (2) with $\Delta L = 0$, it can be seen that the nonlinear control law given by

$$u_{\text{ideal}}(t) = \tilde{\omega}(t)J\omega(t) - JP\omega(t) - J\left[\omega(t)\omega^T(t) + \left(\frac{4K}{1+\|\sigma(t)\|^2} - \frac{\|\omega(t)\|^2}{2}\right)I_3\right]\sigma(t) + 4J\frac{B^T(\sigma(t))}{[1+\|\sigma(t)\|^2]^2}R\sigma(t-\tau) - L^* \quad (30)$$

results in the closed-loop dynamics of the form given in Eq. (5). Because of the restriction of $\|\sigma\| \le 1$, this control law can globally asymptotically stabilize the attitude dynamics given by Eqs. (2) and (4) in the absence of the unmodeled external torque ΔL, as shown in [3,5] for the case when $R = 0$. This assumes that the scalar control gains P, K, and R are selected such that Eq. (5) is stable, and this will in turn be explored in the next section.

Although $u_{\text{ideal}}(t)$ in Eq. (30) is the ideal control law that yields the desired closed-loop dynamics, it cannot be implemented as in Fig. 1 because it cannot be expressed as $u_1(\sigma(t), \omega(t)) + u_2(\sigma(t-\tau))$. Therefore, we consider an alternative control law that is capable of realizing the delayed feedback $u_2(\sigma(t-\tau))$ in actuator 2. This control law is formulated as

$$u(t) = \underbrace{u_1(t)}_{\tilde{\omega}(t)J\omega(t) - JP\omega(t) - J\left[\omega(t)\omega^T(t) + \left(\frac{4K}{1+\|\sigma(t)\|^2} - \frac{\|\omega(t)\|^2}{2}\right)I_3\right]\sigma(t)} + \underbrace{4J\frac{B^T(\sigma(t-\tau))}{[1+\|\sigma(t-\tau)\|^2]^2}R\sigma(t-\tau)}_{u_2(t)} - L^* \quad (31)$$

where the separation into the control forces for actuators 1 and 2 in Fig. 1 is shown and the modeled external torque L^* can be included in either actuator.

Although the stability and performance properties of the closed-loop response are investigated from Eq. (5) [which would require the control law in Eq. (30)], it will be shown that the responses of the system governed by the set of Eqs. (2), (4), and (30) and the set of Eqs. (2), (4), and (31) are almost identical. This is due to the fact that the difference between Eqs. (30) and (31) is of order $\tau\|\sigma\|\|\dot{\sigma}\|$, as can be seen by expanding about $\sigma = 0$ and $\tau = 0$:

$$u(t) - u_{\text{ideal}}(t) \approx 4J\{[1-2\|\sigma(t)\|^2]B^T(\sigma(t)) - [1-2\|\sigma(t-\tau)\|^2]B^T(\sigma(t-\tau))\}R\sigma(t-\tau) + \text{h.o.t.}$$
$$\approx -8J(\tilde{\sigma}(t) - \tilde{\sigma}(t-\tau))R\sigma(t-\tau) + \text{h.o.t.}$$
$$\approx -8JR\tilde{\sigma}(t)\sigma(t-\tau) + \text{h.o.t.} \approx 8JR\tau\tilde{\sigma}(t)\dot{\sigma}(t) + \text{h.o.t.} \quad (32)$$

Thus, for small values of $\|\sigma\|$, $\|\dot{\sigma}\|$, and τ, the difference in the two control laws also remains small, although Eq. (31) is not globally asymptotically stabilizing as is Eq. (30).

It is interesting to compare Eq. (31) with the corresponding Lyapunov-based control law in [3] with an additional linear feedback of the delayed MRP set; i.e.,

$$u_{\mathcal{L}}(t) = \underbrace{\tilde{\omega}(t)J\omega(t) - \mathcal{P}\omega(t) - \mathcal{K}\sigma(t)}_{u_1(t)} + \underbrace{R\sigma(t-\tau)}_{u_2(t)} - L^* \quad (33)$$

Compared with Eq. (33), the controller defined by Eq. (31) has additional nonlinear terms, which allow for the closed-loop behavior to be approximated with linear control theory. This allows for the stability of the closed-loop response to be determined in the frequency domain (as opposed to a Lyapunov–Krasovskii analysis, for instance) and for the feedback gains to be determined from the theory of linear DDEs. Note that all occurrences of the attitude [including inside $B^T(\sigma)$] in $u_2(t)$ are delayed because actuator 2 can only use the delayed signal $\sigma(t-\tau)$ and that, if the control gain R is

set equal to zero, the time delay is removed from the controlled system.

IV. Stability of Closed-Loop Dynamics

Equation (5) is a well-known decoupled DDE with a single point delay [9], and its stability regions in the (K, R, P, τ) space can be obtained analytically for the case in which $P = 0$. In addition, for the case in which $P \neq 0$, various numerical approaches developed in the literature [11,12] may be applied to create stability diagrams in the $K - R$ plane for a given P, for example.

To further analyze the closed-loop dynamics in Eq. (5), the time is nondimensionalized as

$$t^* = \frac{t}{\tau}, \quad \frac{\mathrm{d}}{\mathrm{d}t} = \frac{\mathrm{d}t^*}{\mathrm{d}t}\frac{\mathrm{d}}{\mathrm{d}t^*} = \frac{1}{\tau}\frac{\mathrm{d}}{\mathrm{d}t^*},$$
$$\frac{\mathrm{d}^2}{\mathrm{d}t^2} = \frac{\mathrm{d}t^*}{\mathrm{d}t}\frac{\mathrm{d}}{\mathrm{d}t^*}\left(\frac{1}{\tau}\frac{\mathrm{d}}{\mathrm{d}t^*}\right) = \frac{1}{\tau^2}\frac{\mathrm{d}^2}{\mathrm{d}t^{*2}} \tag{34}$$

Using the transformation given in Eq. (34) in Eq. (5), the latter becomes

$$\sigma'' + \tau P\sigma' + \tau^2 K\sigma = \tau^2 R\sigma(t^* - 1) \tag{35}$$

which, because P, K, and R are scalars, can be written as three second-order scalar DDEs:

$$\sigma_i'' + \bar{P}\sigma_i' + \bar{K}\sigma_i = \bar{R}\sigma_i(t^* - 1), \qquad i = 1, 2, 3 \tag{36}$$

where prime "′" and double prime "″" represent for the first and second derivatives of the MRP σ_i with respect to t^*, respectively, and $\bar{P} = \tau P$, $\bar{K} = \tau^2 K$, and $\bar{R} = \tau^2 R$. Introducing the state-space variables

$$z_1 = \sigma_i, \qquad z_2 = \sigma_i', \qquad i = 1, 2, 3 \tag{37}$$

Eq. (36) can then be written in the state-space form

$$z' = Az(t^*) + Bz(t^* - 1) \tag{38}$$

where

$$z = \begin{Bmatrix} z_1 \\ z_2 \end{Bmatrix}, \qquad A = \begin{pmatrix} 0 & 1 \\ -\bar{K} & -\bar{P} \end{pmatrix}, \qquad B = \bar{R}\begin{pmatrix} 0 & 0 \\ 1 & 0 \end{pmatrix} \tag{39}$$

Two methods, an analytical approach and a numerical approach, are further implemented to study the stability of the closed-loop system of Eq. (38). The analytical stability approach only applies to the case of no derivative feedback control with $\bar{P} = 0$.

A. Analytical Stability for No Derivative Feedback Control

Setting $\bar{P} = 0$ in Eq. (36), its corresponding characteristic equation can be written as

$$s^2 + \bar{K} - \bar{R}e^{-s} = 0 \tag{40}$$

Because unstable systems have eigenvalues with positive real parts, s must be set equal to zero and $i\omega$ to obtain stability boundaries. If one sets $s = 0$, Eq. (40) yields the divergence stability boundary as

$$\bar{K} = \bar{R} \tag{41}$$

whereas setting $s = j\omega$ for $\omega \in \mathbb{R}$ and separation of the real and imaginary parts yields

$$-\omega^2 + \bar{K} - \bar{R}\cos\omega = 0, \quad \bar{R}\sin\omega = 0 \tag{42}$$

The second equation in Eq. (42) yields

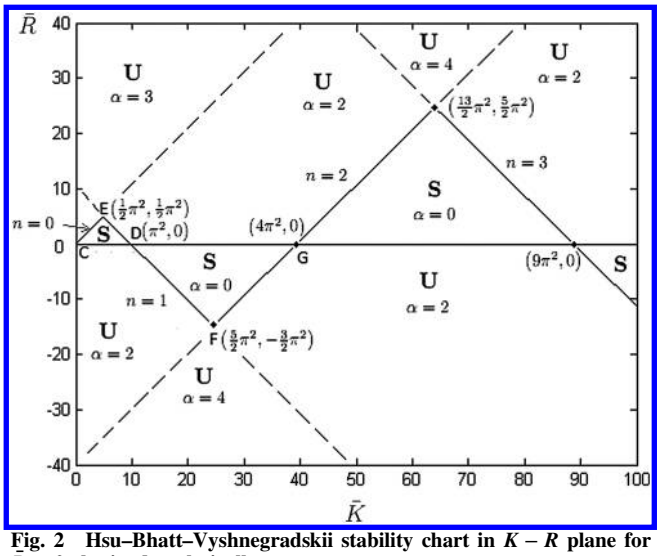

Fig. 2 Hsu–Bhatt–Vyshnegradskii stability chart in $K - R$ plane for $\bar{P} = 0$ obtained analytically.

$$\sin\omega = 0, \quad \text{or} \quad \bar{R} = 0 \tag{43}$$

Solving Eqs. (42) and (43) simultaneously yields the flutter (Hopf) stability boundaries as

$$D = D_1 \cup D_2 \tag{44}$$

where

$$D_1 = \{(\bar{K}, \bar{R}) | \bar{R} = 0, \bar{K} > 0\},$$
$$D_2 = \{(\bar{K}, \bar{R}) | \bar{K} - \bar{R}(-1)^n = n^2\pi^2\}, \qquad n = 0, 1, 2, \cdots \tag{45}$$

The corresponding stability chart in the normalized $(\bar{K}, \bar{R})$ plane, which is shown in Fig. 2, is known as the Hsu–Bhatt–Vyshnegradskii stability chart in the literature [9]. The stable (S) and unstable (U) regions are shown in Fig. 2 along with the numbers α of unstable roots of Eq. (40) in each region. The divergence boundary with slope $+1$ through the origin corresponds to a difference of ± 1 between the values of α in adjacent regions, whereas the remaining flutter (Hopf) boundaries correspond to a difference of ± 2 between the values of α in adjacent regions.

Corollary: The trivial solution of the DDE (36) is exponentially asymptotically stable if and only if there exists an integer $n_1 \geq 0$ such that either

$$\bar{R} > 0, \qquad \bar{R} < \bar{K} - (2n_1)^2\pi^2, \quad \text{and} \quad \bar{R} < -\bar{K} + (2n_1 + 1)^2\pi^2 \tag{46}$$

or

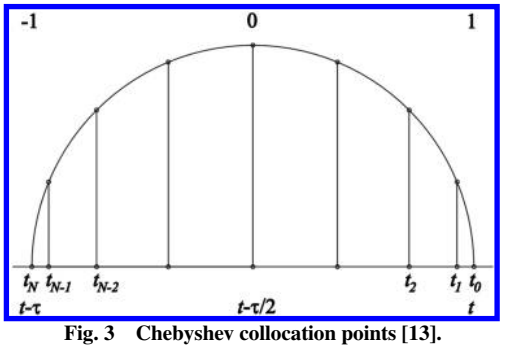

Fig. 3 Chebyshev collocation points [13].

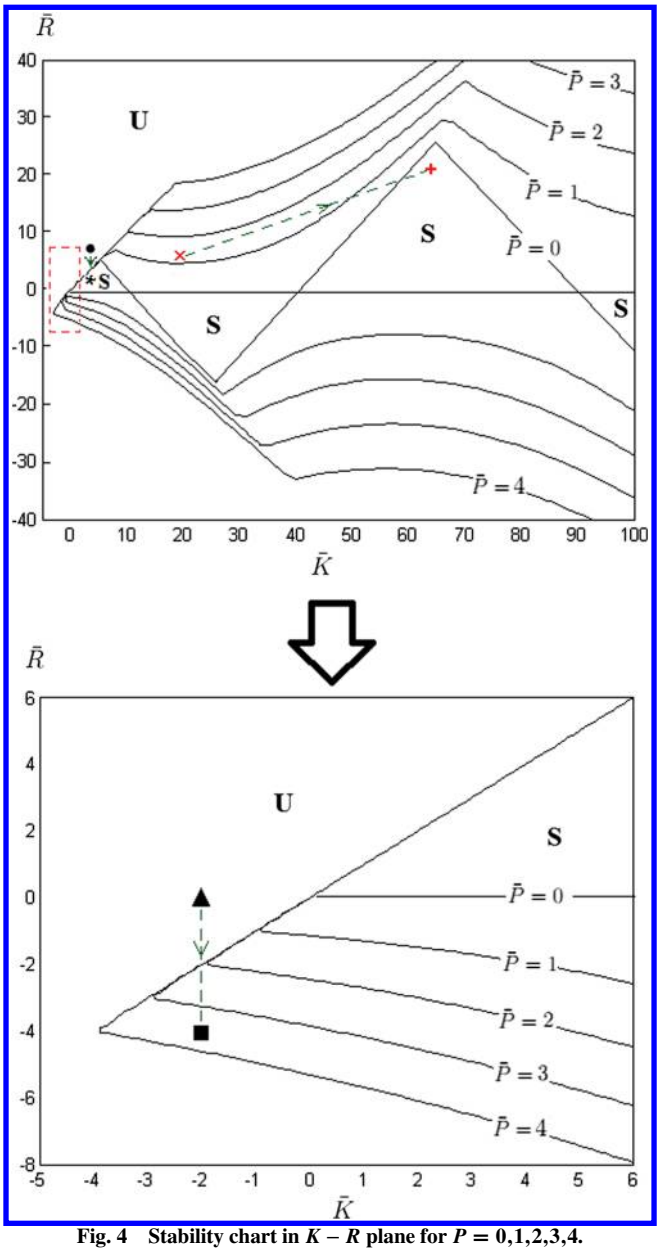

Fig. 4 Stability chart in $K-R$ plane for $P=0,1,2,3,4$.

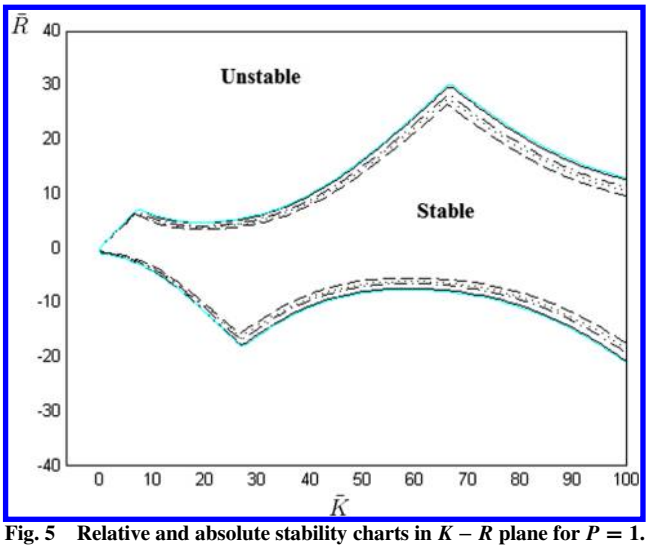

Fig. 5 Relative and absolute stability charts in $K-R$ plane for $P=1$. The spectral abscissae for the relative stability boundaries are -0.01 (solid line), -0.05 (dashed dotted line), -0.07 (dotted line), and -0.1 (dashed line).

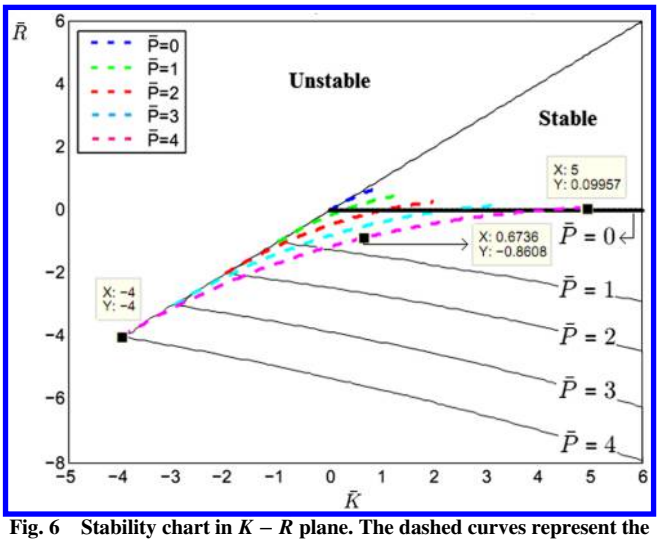

Fig. 6 Stability chart in $K-R$ plane. The dashed curves represent the loci of the parameter sets corresponding to the critically damped cases for different values of $\bar{P}$.

$$\bar{R}<0, \quad \bar{R}>-\bar{K}+(2n_1+1)^2\pi^2, \quad \text{and} \quad \bar{R}>\bar{K}-(2n_1+2)^2\pi^2 \tag{47}$$

Proof: Because the divergence boundary $\bar{K}=\bar{R}$ is delay independent [10], for the system without the time delay, Eq. (42) becomes

$$s^2=\bar{R}-\bar{K} \tag{48}$$

which results in the stable behavior for $0\le\bar{R}<\bar{K}$ for the system with $\bar{P}=0$. Hence, the region inside the triangle ΔCDE is stable. On the other hand, by crossing through the divergence and Hopf stability boundaries, the number of unstable characteristic exponents, α, increases by one and two, respectively (see Fig. 2). Because inside ΔCDE is stable with $\alpha=0$, starting from a point inside this triangle, if we cross through segment CD (which is the Hopf stability boundary) toward outside of that triangle, the parameter α increases by two, which means that we are in the unstable region. Now, if we move from a point on this unstable region toward the inside of ΔDFG by crossing the segment DF, α decreases by two again and becomes zero, which implies that inside ΔDFG is also stable. The same strategy can be followed for the other triangles. □

The first set of conditions given in the corollary (Eq. 46) gives the stable triangles above the $\bar{R}$ axis, whereas the second set (Eq. 47) produces the stable triangles below that axis. Figure 2 represents the stability chart obtained analytically in the $\bar{K}-\bar{R}$ plane. The intersections of the first three consequent pairs of lines given in the set D_2 in Eq. (45) are obtained analytically and represented in Fig. 2 along with the crossing points of the lines with the $\bar{K}$ axis.

B. Numerical Stability Analysis for General Case

For the case $\bar{P}\neq 0$, the characteristic equation is

$$s^2+\bar{P}s+\bar{K}-\bar{R}e^{-s}=0 \tag{49}$$

which, after setting $s=j\omega$ and separating the real and imaginary parts, yields

$$-\omega^2+\bar{K}-\bar{R}\cos\omega=0, \quad \bar{P}\omega+\bar{R}\sin\omega=0 \tag{50}$$

Table 1 Parameter values [3]

Parameter	Value
J	$\text{diag}[30 \quad 20 \quad 10]\ \text{kg} \cdot \text{m}^2$
$\sigma(t_0)$	$[-.3 \quad -.4 \quad .2]^T$
$\omega(t_0)$	$[.2 \quad .2 \quad .2]^T$

It can be seen that the flutter stability boundaries for this case do not remain as straight lines. However, like the case in which $\bar{P} = 0$, the $\bar{K} = \bar{R}$ line can still be seen to correspond to the divergence (fold) instability. We now describe a numerical method called the Chebyshev spectral continuous time approximation (CSCTA), which is used to investigate the stability of this case.

Chebyshev collocation points can be introduced as the projections of the equispaced points on the upper half of the unit circle onto the horizontal axis. In the CSCTA method, the interval $[x(t-\tau), x(t)]$ is broken into $N = m - 1$ subintervals, the lengths of which are determined based on the positions of Chebyshev collocation points, in which m is the number of Chebyshev collocation points. The scaling factor $\frac{2}{\tau}$ is then used to project the interval $[-1, 1]$ onto $[t-\tau, t]$. The Chebyshev meshing points can be obtained by dividing the interval $[t-\tau, t]$ into segments $[t_\alpha, t_{\alpha-1}]$, as illustrated in Fig. 3 [13], in which $t_0 = t$ and

$$t_\alpha = t - \frac{\tau}{2}\left(1 - \cos\frac{\alpha\pi}{N}\right), \qquad \alpha = 1, 2, \cdots, N \tag{51}$$

Note that $\tau = 1$ after the transformation made in Eq. (34).

A Chebyshev spectral differentiation matrix D is defined as

$$D_{11} = \frac{2N^2+1}{6} = -D_{N+1,N+1}, \qquad D_{\beta\beta} = -\frac{t_\beta}{2(1-t_\beta^2)},$$
$$\beta = 2, \cdots, N \quad D_{\alpha\beta} = \frac{c_\alpha(-1)^{\alpha+1}}{c_\beta(t_\alpha - t_\beta)}, \qquad \alpha \neq \beta, \tag{52}$$
$$\alpha, \beta = 1, 2, \cdots, N+1, \qquad c_\alpha = \begin{cases} 2, & \alpha = 1, N+1 \\ 1, & \text{otherwise} \end{cases}$$

Now, if the equation of motion is written in the state-space form as in Eq. (38), then based on the definition for the augmented vector $\mathcal{Y}$

$$\mathcal{Y} = [z^T(t_0) \quad z^T(t_1) \quad z^T(t_2) \quad \cdots \quad z^T(t_N)]^T,$$
$$\alpha = 0, 1, \cdots, N \tag{53}$$

where $t_0 = t$ and $t_N = t - \tau$ from Fig. 3, the infinite-dimensional DDE system in Eq. (38) can be approximated as a large-dimensional set of ordinary differential equations. That is,

$$\dot{\mathcal{Y}} = \mathcal{A}\mathcal{Y} \tag{54}$$

where [11,12]

$$\mathcal{A} = \begin{bmatrix} A & 0 & \cdots & 0 & B \\ & & \frac{2}{\tau}[\mathbb{D}]^{q+1,mq} & & \end{bmatrix} \tag{55}$$

is the discretized infinitesimal generator of the solution operator corresponding to Eq. (54), where $\tau = 1$, $q = 2$, and

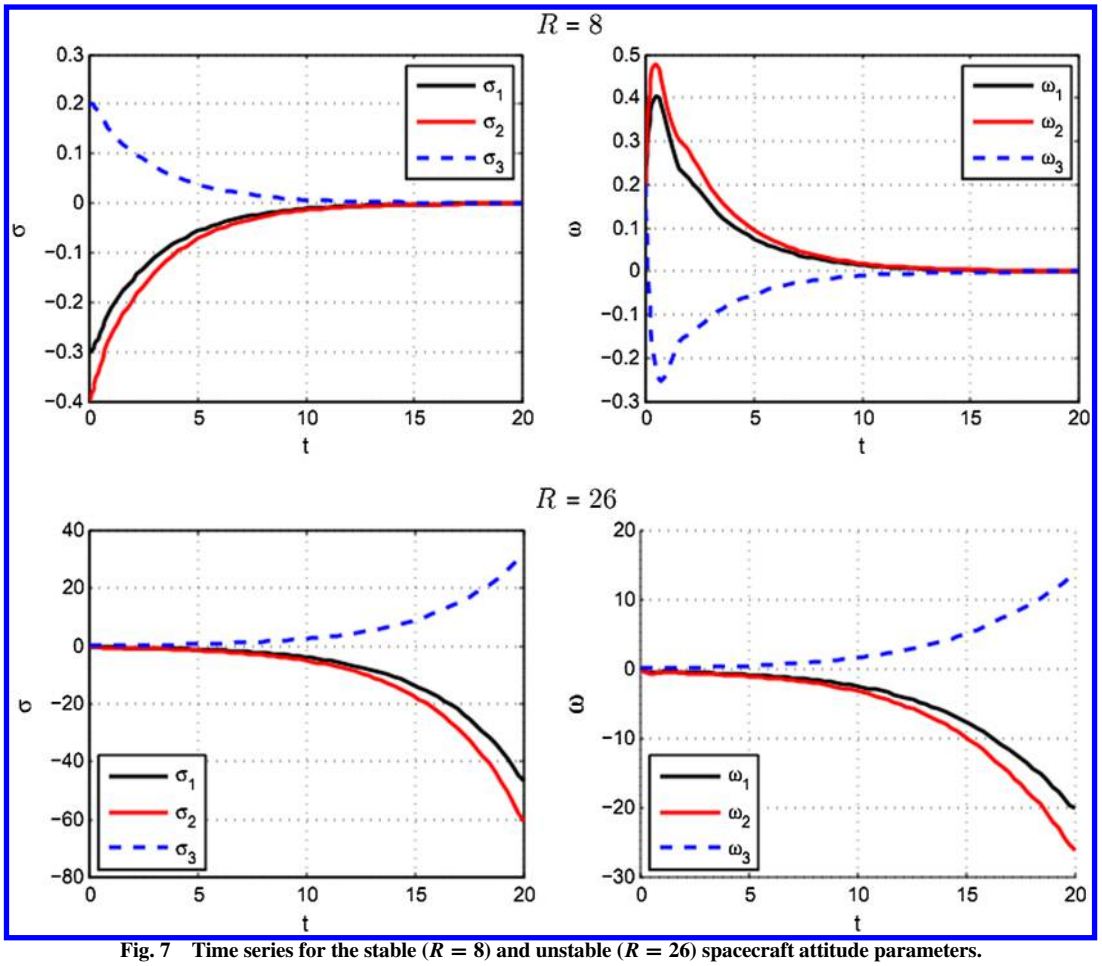

Fig. 7 Time series for the stable ($R = 8$) and unstable ($R = 26$) spacecraft attitude parameters.

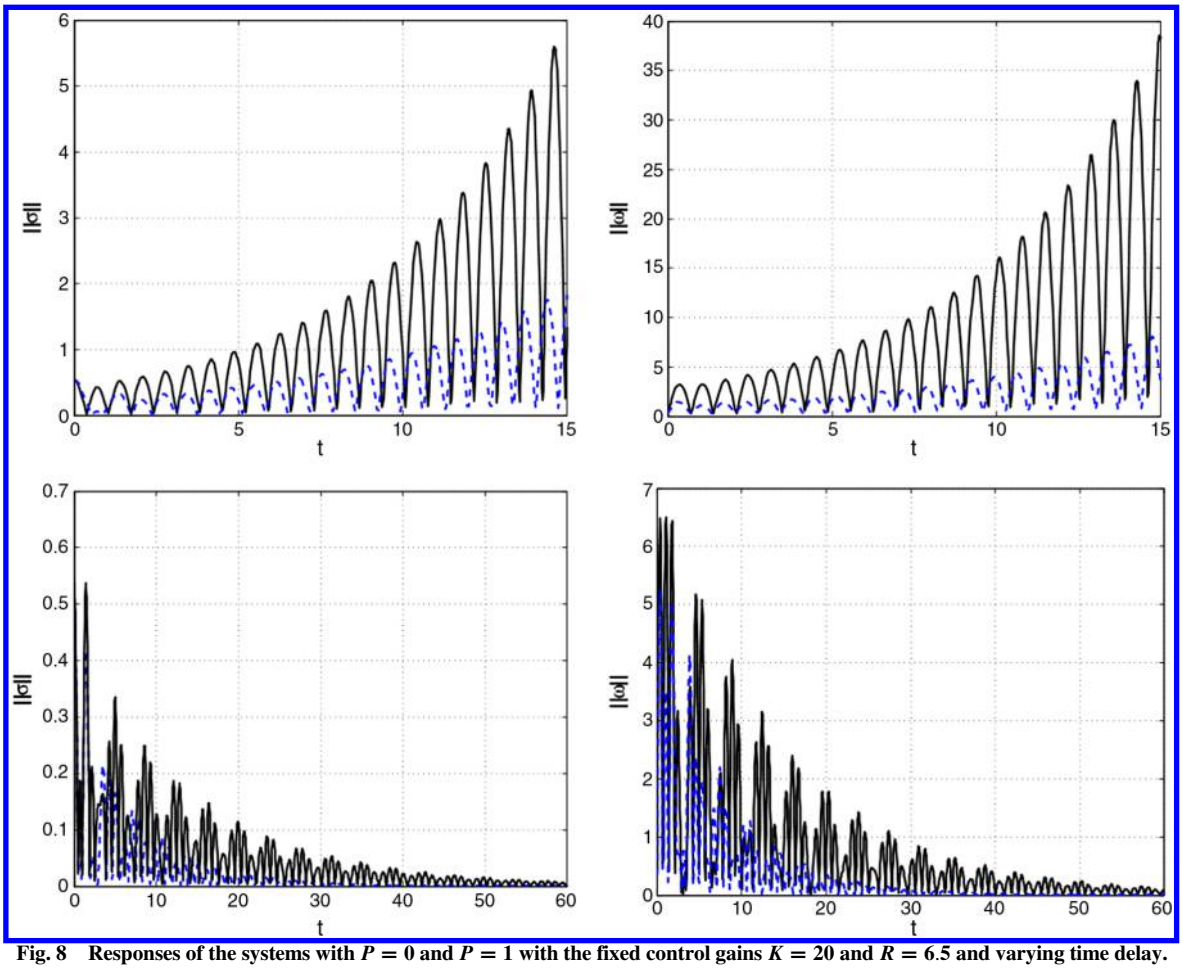

Fig. 8 Responses of the systems with $P = 0$ and $P = 1$ with the fixed control gains $K = 20$ and $R = 6.5$ and varying time delay.

$$\mathbb{D}_{mq\times mq} = D_{m\times m} \otimes I_{q\times q} \tag{56}$$

in which only rows of $\mathbb{D}$ between $q+1$ and mq enter in the $mq \times mq$ matrix $\mathcal{A}$. Based on the left half-plane analysis, the real parts of the eigenvalues of the matrix $\mathcal{A}$ in Eq. (55) determine the stability of the system such that, if all eigenvalues of matrix $\mathcal{A}$ have negative real parts, then the system is asymptotically stable. The results shown in Fig. 4 are obtained analytically for $\bar{P} = 0$ and numerically using CSCTA for $\bar{P} > 0$. 85 Chebyshev collocation points are used in CSCTA in a 50×50 mesh grid so that the dimension of $\mathcal{A}$ is 170×170. The scripts S and U in the figure refer to the stable and unstable regions, respectively. The enlarged view of the region inside the dashed rectangle in the upper figure is shown in the lower figure. The *, •, ×, +, ▲, and ■ represent the parameters used later in the simulations.

We now consider the problem of delay stabilization of an otherwise unstable nondelayed system by increasing either the gain of the delayed actuator or the time delay itself. The magnification of the small region shown by dashed rectangle in Fig. 4 illustrates how increasing the gain of the delayed actuator stabilizes an otherwise unstable system when $\bar{K} < 0$ (consequently, when $K < 0$). The behavior of the system in the $\bar{K} - \bar{R}$ plane is plotted in Fig. 4 for different values of $\bar{P}$ in the system (36). As mentioned before, the stability boundaries do not remain straight lines for the $P \neq 0$ cases except for the $\bar{R} = \bar{K}$ divergence boundary.

It should be noted that, if system is just barely stable, then a small error or uncertainty in the system parameters could push the system over the stability boundary. Hence, it is often desired to design systems with some margin of error. The relative stability is compared with the stability boundary for $\bar{P} = 1$, for instance, in the $\bar{K} - \bar{R}$ plane, as shown in Fig. 5. For the relative stability boundary in the figure, the spectral abscissae are assumed to be equal to −0.01, −0.05, −0.07, and −0.1.

V. Gain Selection for Critically Damped Response

It is often desired for the system to behave in a critically damped manner in which two roots meet on the real axis in the s plane right before their imaginary parts become nonzero. To achieve this specified performance, the characteristic (exponential) polynomial of the normalized delayed system should be solved simultaneously along with its derivative taken with respect to the polynomial variable, s. Therefore, we have the following set of two equations:

$$q(s) = s^2 + \bar{P}s + \bar{K} - \bar{R}e^{-s} = 0 \tag{57a}$$

$$f(s) = \frac{\mathrm{d}q}{\mathrm{d}s} = 2s + \bar{P} + \bar{R}e^{-s} = 0 \tag{57b}$$

The location of the common zeros of $q(s)$ and $f(s)$ in the s plane determines the system behavior in the critically damped case. Each curve in Fig. 6 is obtained by solving $\bar{R}$ and $\bar{K}$ for a range of negative real values of s for a given $\bar{P}$. If one eliminates $\bar{R}$ from Eq. (57a) by substituting it from Eq. (57b), a second-order polynomial can be obtained for which the solution for a repeated root of s, for a given $\bar{P}$, determines the conditions

$$\bar{K} = \left(\frac{\bar{P}}{2} + 1\right)^2 - \bar{P}, \qquad \bar{R} = 2e^{-\left(\frac{\bar{P}}{2}+1\right)} \tag{58}$$

which represent a point that is located at the tip of each dashed curve shown in Fig. 6.

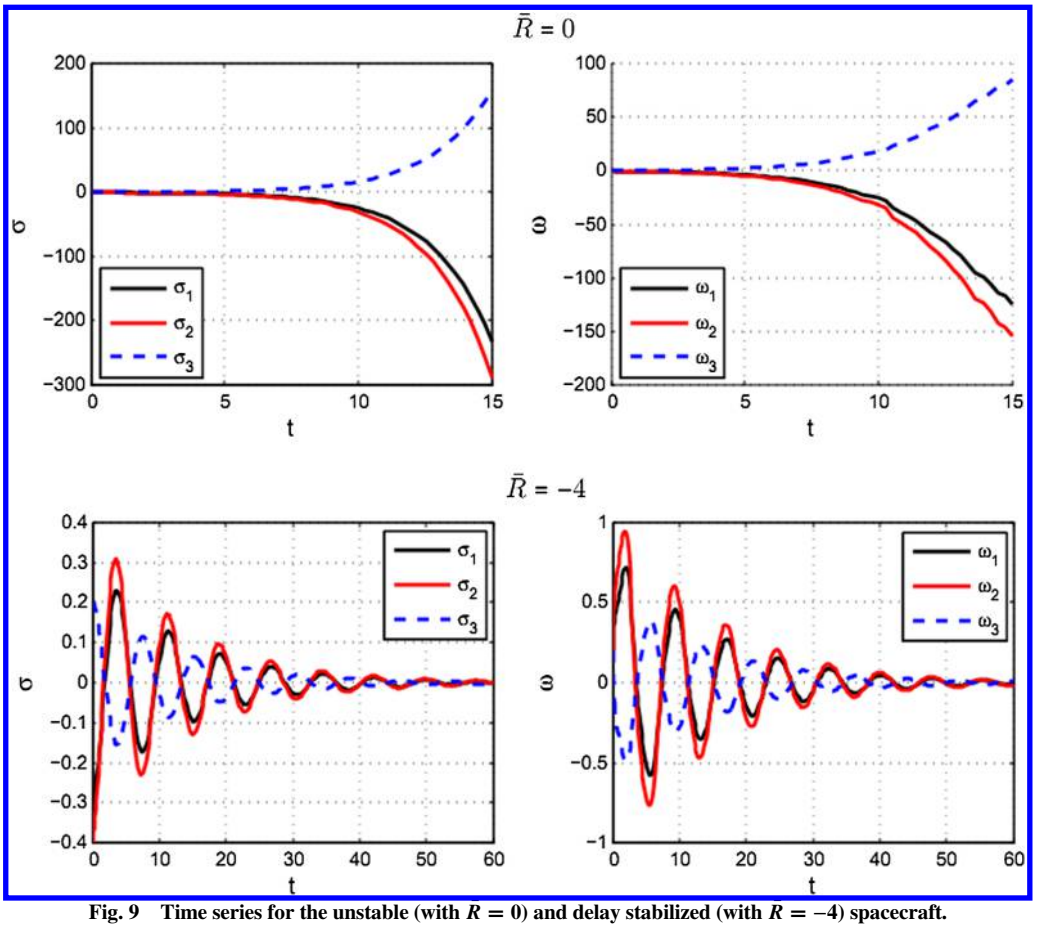

Fig. 9 Time series for the unstable (with $R = 0$) and delay stabilized (with $R = -4$) spacecraft.

VI. Integral Feedback to Eliminate Steady-State Error

In the case an unmodeled torque ΔL is present, which is constant or changing vary slowly, the attitude will exhibit a nonzero steady-state error, which is not desired. This error can be obtained implicitly as

$$\sigma_{SS} = \frac{B(\sigma_{SS})J^{-1}\Delta L}{4(K - R)} \tag{59}$$

To eliminate this error, an integral feedback term is added to the desired closed-loop dynamics of the system. Therefore, the new closed-loop dynamics are

$$\ddot{\sigma} + P\dot{\sigma} + K\sigma + K_i \int_0^t \sigma(\eta)\,\mathrm{d}\eta = R\sigma(t - \tau) \tag{60}$$

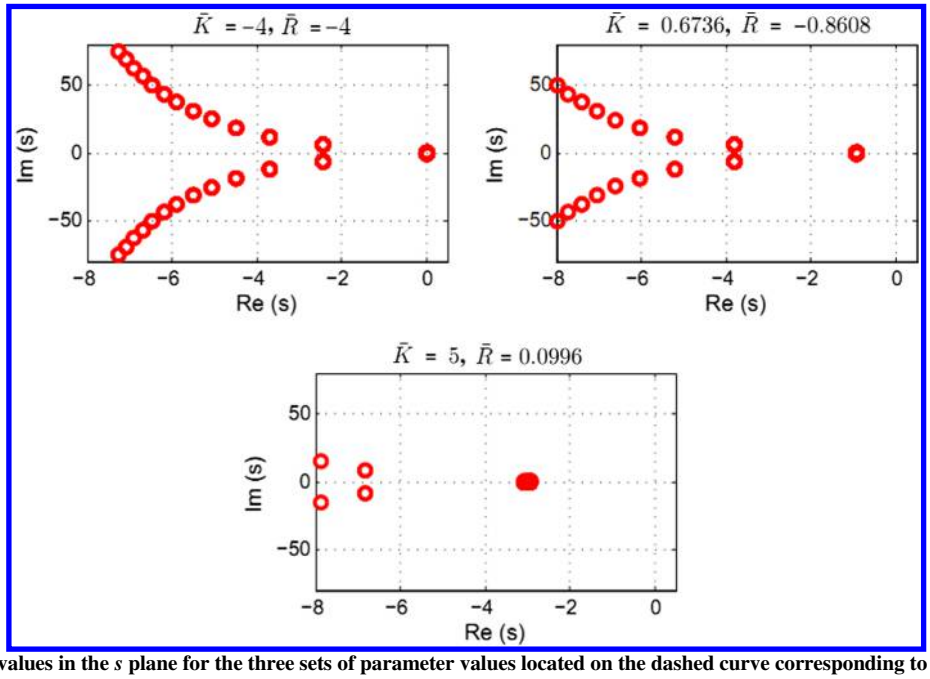

Fig. 10 Eigenvalues in the s plane for the three sets of parameter values located on the dashed curve corresponding to $\bar{P} = 4$ in Fig. 6.

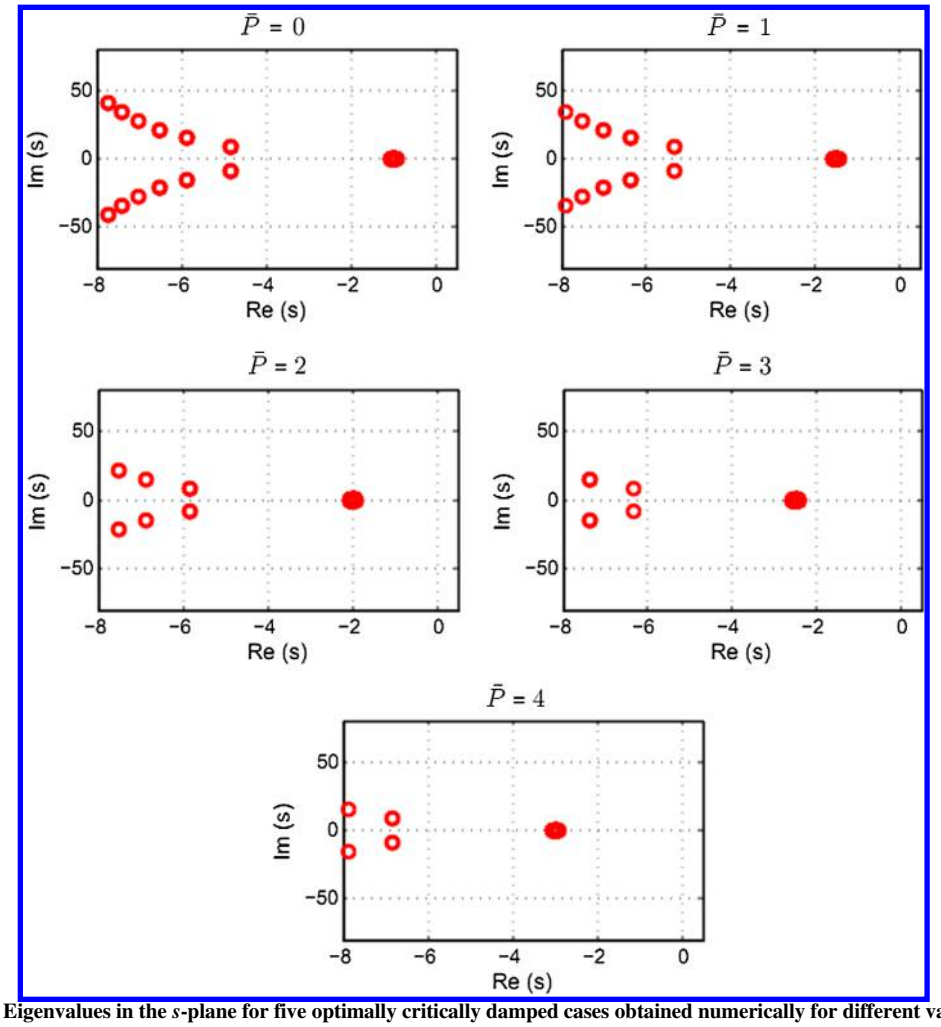

Fig. 11 Eigenvalues in the *s*-plane for five optimally critically damped cases obtained numerically for different values of $\bar{P}$.

where, compared to the desired closed-loop dynamics in Eq. (5), the additional feedback integral term in the left-hand side of the equation is to compensate for the steady-state error due to the unmodeled torque ΔL. The integral gain K_i in Eq. (60) is selected to be smaller than the proportional, K, and the derivative, P, gains because it is not preferable for the damping properties of the system or the frequency of oscillations to change drastically.

Following similar steps in the inverse dynamics approach as those shown in the proof of the lemma in Sec. III, it can be easily shown that the additional integral feedback term in the closed-loop dynamics (60) corresponds to a supplementary control force of

$$u_{\text{supp}}(t) = -4JK_iB^{-1}(\sigma(t))\int_0^t \sigma(\eta)\,\mathrm{d}\eta \tag{61}$$

in Eq. (31), which now becomes a proportional-integral-derivative (PID)-type control law. The supplemental integral term $u_{\text{supp}}(t)$ can be added to either the nondelayed actuator or the delayed actuator.

It is instructive to compare our controller with the standard MRP-based control law

$$u_{\mathcal{L}}(t) = \tilde{\omega}(t)J\omega(t) - P\omega(t) - K\sigma(t) + R\sigma(t-\tau) - PK_iz(t) - L^*$$
$$z(t) = \int_0^t (K\sigma(\eta) + J\dot{\omega}(\eta))\,\mathrm{d}\eta \tag{62}$$

obtained using the Lyapunov function [3]

$$V(\omega) = \frac{1}{2}\omega^TJ\omega + 2K\,\ln(1+\sigma^T\sigma) + \frac{1}{2}z^TK_iz \tag{63}$$

with the extra linear delayed feedback term added into the control law. However, even with $R = 0$, the resulting closed-loop dynamics

$$J\dot{\omega} + P\omega + K\sigma + PK_iz = 0 \tag{64}$$

are not linear due to the nonlinearities in Eq. (4), although for small motions, $B(\sigma)$ can be linearized to yield linear closed-loop dynamics. On the other hand, the inverse-dynamics-based control law given in Eq. (31), along with the supplementary term $u_{\text{supp}}(t)$ given in Eq. (61), directly results in the linear delay integrodifferential equation for the closed-loop dynamics shown in Eq. (60).

VII. Simulation Results

In this section, we study the effect of the proposed controller via simulations of the closed-loop DDE using MATLAB dde23. Specifically, the time histories for certain stable and unstable locations in the stability chart for the closed-loop system are produced for the time-delayed system corresponding to the parameters in Table 1. First, two points, one from the stable region shown with * and the other one from the unstable region shown with •, are selected arbitrarily from the regions of stability and instability shown in Fig. 4. The response is plotted in Fig. 7 for $P = 8$, and $K = 16$, and time delay $\tau = 0.5$ s for the stable and unstable points indicated by * and • in Fig. 4. In Fig. 7, MRPs are shown in left and angular velocity components are shown in right. The initial conditions for this figure are given in Table 1. It is seen that the stability of the simulated response agrees with the corresponding location of the parameter values on the stability diagram.

To study the delay stabilization strategy by varying τ, we fix the control gains K and R as well as the dimensionless control gain $\bar{P}$.

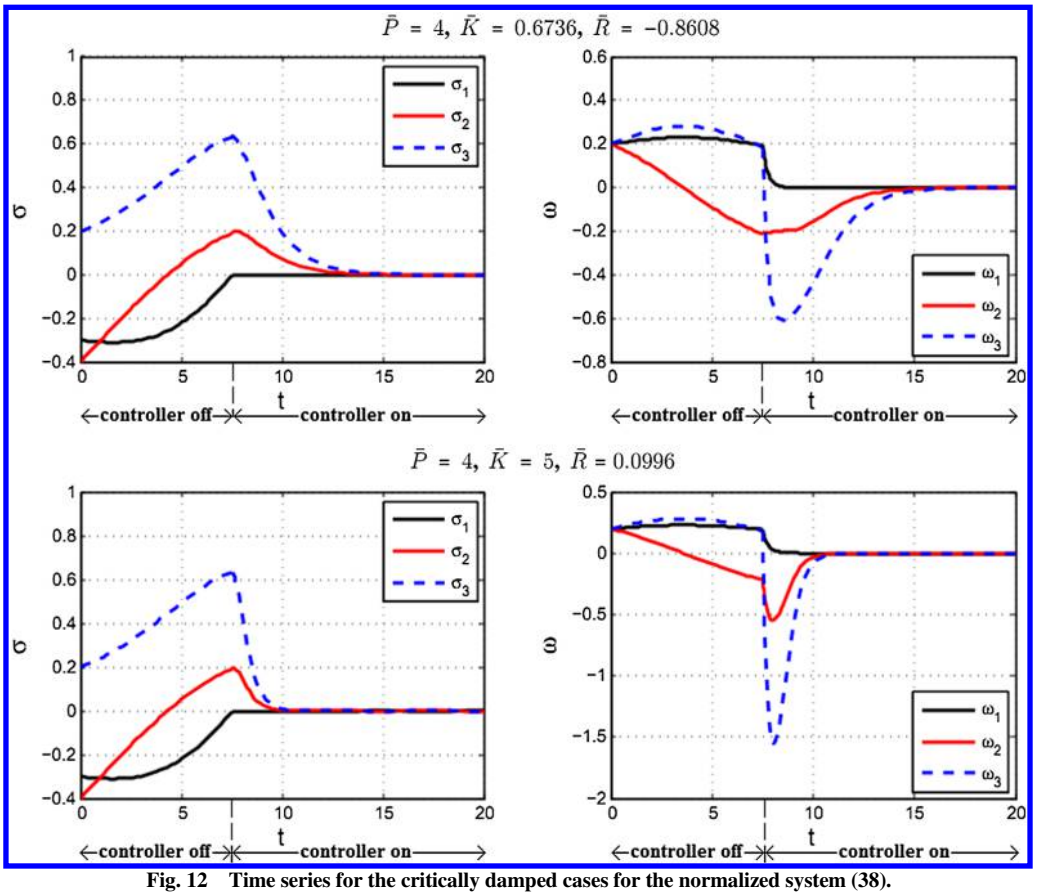

Fig. 12 Time series for the critically damped cases for the normalized system (38).

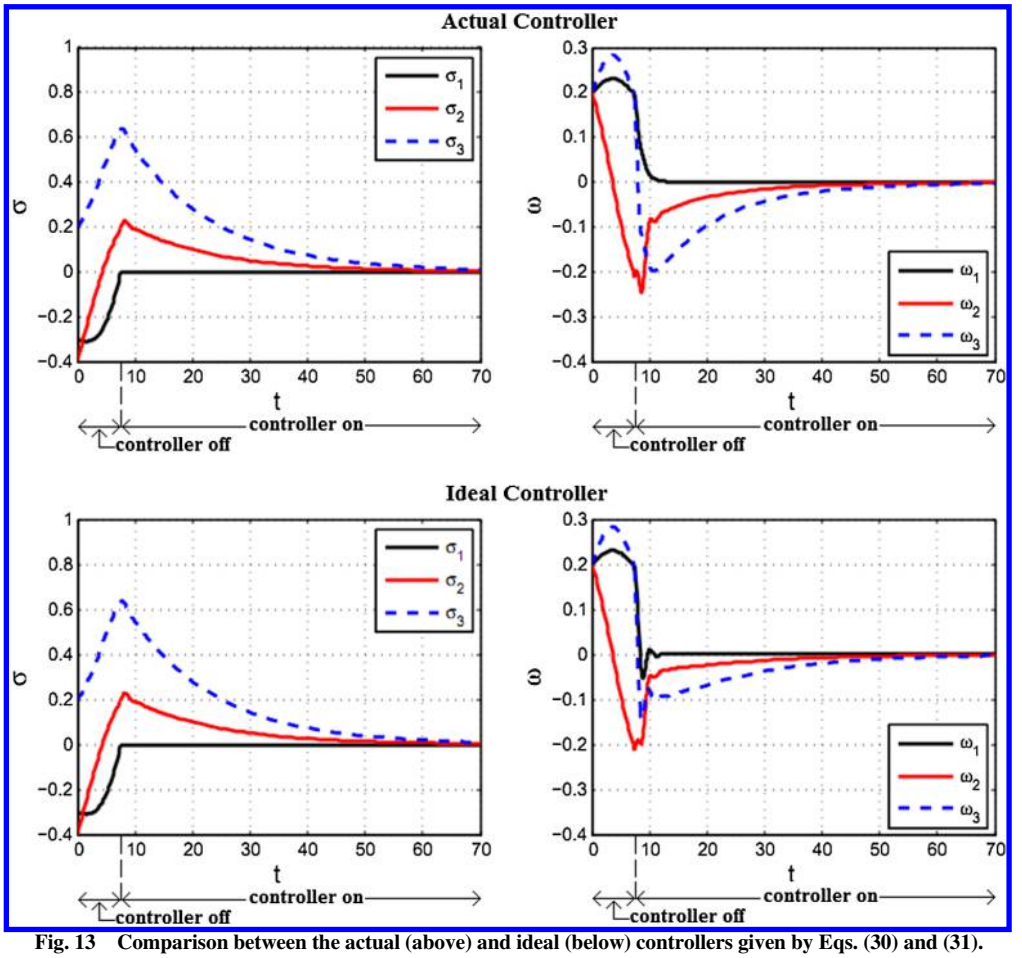

Fig. 13 Comparison between the actual (above) and ideal (below) controllers given by Eqs. (30) and (31).

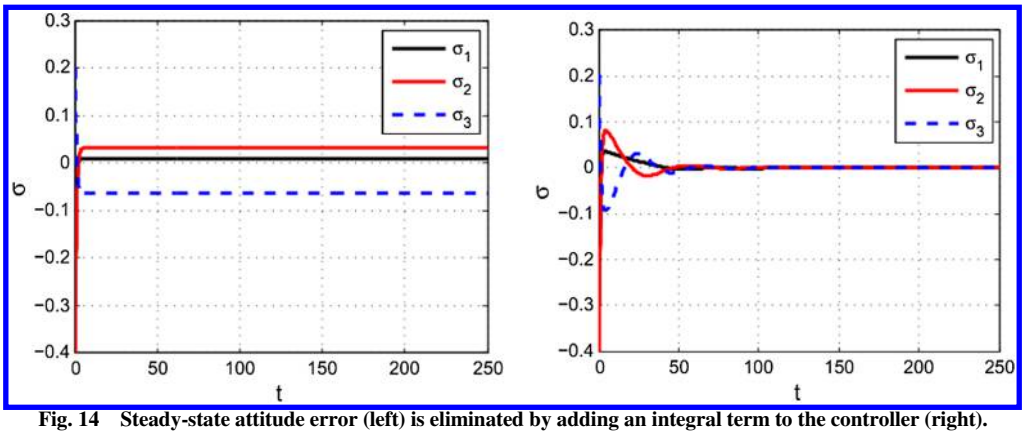

Fig. 14 Steady-state attitude error (left) is eliminated by adding an integral term to the controller (right).

Then, we select a point inside the unstable region such that a line that connects that point to the origin in the $\bar{K} - \bar{R}$ parameter plane passes through the neighboring stable region on the right. Next, we let the time delay increase from the initial value $\tau = 1$ s such that the unstable point moves into the neighboring stable region on the right. Note that actuator 2 has an unavoidable minimum time delay such that, whereas the time delay can be increased artificially by feeding back the states at previous times, it is impossible to reduce the delay from the given minimum value. The selected values for K and R are $K = 20$ and $R = 6.5$. The unstable point corresponding to these values of K and R when $\tau = 1$ s is shown by $\times$ in Fig. 4. Following the delay stabilization strategy, we increase τ to $\tau = 1.7748$ s in order to let the unstable point move into the neighboring stable region. The corresponding stable point is shown by $+$ in Fig. 4. Note that, when $\bar{P} \neq 0$, in order to fix $\bar{P} = \tau P$, we need to change the control gain P accordingly as τ changes. In Fig. 8, unstable responses are shown in the first row for $\bar{P} = 0$ (solid line) and $\bar{P} \neq 0$ (dashed line) for the point $(\bar{K}, \bar{R}) = (20, 6.5)$ corresponding to $\tau = 1$ s shown by $\times$ in Fig. 4. Stable responses are shown in the second row of the figure for $\bar{P} = 0$ (solid line) and $\bar{P} \neq 0$ (dashed line) for the point $(\bar{K}, \bar{R}) = (63, 20.47)$ corresponding to $\tau = 1.7748$ s shown by $+$ in Fig. 4. The initial conditions are given in Table 1. It can be seen that the response of the system with $\bar{P} = 1$ converges to zero faster than that with $\bar{P} = 0$, as expected.

To address delay stabilization by increasing the gain of the delayed actuator, simulations are performed for the non-delayed system with $\bar{R} = 0$ as well as the delayed system with $\bar{R} = -4$. The corresponding results are shown in Fig. 9 with normalized control gains $\bar{P} = 4$ and $\bar{K} = -2$ for the unstable and stable points indicated respectively by ▲ and ■ in Fig. 4. MRPs are shown in left and angular velocity components are shown in right. The initial conditions for this figure are given in Table 1. The results in Fig. 9 agree with the stability chart given in Fig. 4. Recall that the normalized control gains correspond to Eq. (36) when the time delay is normalized to one. Thus, when the gain of the nondelayed actuator is for some reason constrained to value(s) that result in an unstable closed-loop system the strategy of delay stabilization can be practically implemented by increasing the gain of the delayed actuator to an appropriate level.

Next, we monitor the behavior of the system by starting from the point $\bar{K} = \bar{R} = -4$, at the corner of the stable region corresponding to the $\bar{P} = 4$, where the divergence and flutter boundaries meet. We move along the dashed curve obtained by Eq. (57) in Fig. 6 toward the right end of the curve while $\bar{P} = 4$. Figure 10 shows the loci of eigenvalues for the three points indicated in Fig. 6. The eigenvalues' loci of the system in the optimally critically damped case (second row in Fig. 10) obtained in Eq. (58) suggest the best choice of the parameter set for the long-term behavior of the system. In Fig. 11, the eigenvalues of the system are studied at the optimally critically damped scenarios expressed in Eq. (58) for different values of $\bar{P}$. These five scenarios correspond to the parameter sets located at the right end of the dashed curves shown in Fig. 6 and are obtained via Eq. (58). We call these points optimally critically damped because their dominant negative real eigenvalues are further to the left compared to those of the other critically damped points, as a result of which the system attitude orientations and the angular velocities damp out faster. Consequently, the first negative real eigenvalue shifts further to the left as $\bar{P}$ increases. The repeated real eigenvalues can be found in Figs. 10 and 11. The time series corresponding to the critically damped performance are shown in Fig. 12, in which the controller is turned off for the first 7.5 s and is then turned on for two of the parameter sets indicated by ■ in Fig. 6. For each parameter set, MRPs (left) and angular velocities (right) are shown. The initial conditions for the figure are given in Table 1. It can be seen in the figure that for $\bar{P} = 4$ (corresponding to $\bar{K} = 5$ and $\bar{R} = 0.0996$) the system damps out faster.

So far, the simulations have been based on the actual control law defined in Eq. (31), whereas the stability diagrams are obtained for the closed-loop dynamics given in Eq. (5), which are the result of using the ideal control law proposed in Eq. (30). To justify the control law in Eq. (31), we simulate the controlled system with the two different control laws introduced in Eqs. (30) and (31) for a variety of sets of control gains $\bar{P}$, $\bar{K}$, and $\bar{R}$. It can be seen that the time histories of the system attitude and angular velocities controlled by these controllers are practically identical. The reason for this is that, by neglecting the second-order delayed terms as compared to the first-order terms in the actual control law proposed in Eq. (31), the ideal control law given in Eq. (30) can be obtained with a good approximation. To compare these two control laws, we numerically integrate the system obeying each of these control laws. In Fig. 13 the attitude orientations and angular velocities of the controlled system are plotted for $\bar{P} = 1$, $\bar{K} = 2.2$, and $\bar{R} = 2$ using the two controllers with the controllers being turned on after 7.5 s. The initial conditions for the figure are given in Table 1. As shown in the figure, the MRPs behave identically in both cases, whereas the angular velocities behave not identically but very similarly.

To study the effect of adding the integral term to the controller, the response of the system is studied with the unmodeled torque $\Delta L = [5, 10, -10]^T$ N · m, which is, in point of fact, much larger than what spacecraft would normally experience. In Fig. 14, the preceding control law given in Eq. (31) is applied to the system on the left, whereas the supplementary $u_{\text{supp}}(t)$ term given in Eq. (61) is added to the controller for the system on the right. The steady-state attitude offset in Fig. 14 is due to unmodeled external torque $\Delta L = [5, 10, -10]^T$ and is obtained via Eq. (59) as $\sigma_{\text{SS}} = [0.0107, 0.0322, -0.0644]^T$. The normalized control gains for both plots on the left and the right are $\bar{P} = 4$, $\bar{K} = 5$, and $\bar{R} = 0.0996$. The integral gain for the plot on the right is $K_i = -0.03$. Initial conditions are given in Table 1. Note that, once a proper K_i is selected, it would be capable of eliminating the steady-state error due to any unmodeled torque. Another important observation is that the steady-state error decreases as the proportional gain K ncreases.

It should be mentioned here that the norm of the MRP set was always less than one, and hence, there was no need to switch to the shadow set in the simulations. According to the negligible difference between the ideal and actual control laws shown in Eqs. (30) and (31) and the simulation results, it can be seen that the multiactuator PID

control law obtained by adding the supplementary term in Eq. (61) to the control law given in Eq. (31) results in asymptotic stability of the system described by Eqs. (2) and (4) for sufficiently small τ, $\|\sigma\|$, and $\|\dot{\sigma}\|$.

VIII. Conclusions

In this paper, a nonlinear delayed multiactuator control law has been introduced to attain the desired closed-loop dynamics of a rigid spacecraft by following the inverse dynamics approach used in previous literature. As opposed to the authors' prior work in which the time delay was assumed in the measurements, the time delay here has been assumed to be in one of the actuators whereas the other is nondelayed. The stability of the multiactuator closed-loop control was shown to approximately reduce to the stability of a linear second-order delay differential equation for which the Hsu–Bhatt–Vyshnegradskii stability chart can be used to select a stable set of control gains given the time delay. The approach could possibly be extended for use in desaturation maneuvers involving two different types of actuators, although the current formulation does not take internal momentum management into account.

Note that the linear closed-loop dynamics is the result of a rigorous ideal nonlinear control obtained by the inverse dynamics approach and thus retains the almost global nonlinear stability results. This contrasts sharply from developing linearized closed-loop dynamics, which are only valid in a local neighborhood, and doing a local stability analysis. The only caveat is that the error between the ideal and actual controllers is of order $\tau\|\sigma\|\|\dot{\sigma}\|$, so that the actual law is not globally asymptotically stabilizing because this strategy assumes $\|\sigma\|$, $\|\dot{\sigma}\|$, and τ to be small enough. Also, note that no system properties, such as inertia, are included in the controlled closed-loop system, a property beneficial in adaptive control strategies. Delay stabilization was also investigated, in which either the gain of the actuator with a time delay is intentionally increased or the time delay is intentionally increased in order to stabilize the closed-loop dynamics, which would be unstable without delay due to constraints in the gain of the nondelayed actuator. One practical way to increase the time delay would be to feed back the states at the previous time. In the simulations, the control gains K and R were fixed as well as the dimensionless derivative control gain $\bar{P}$, and the time delay was allowed to increase such that the unstable parameter set moves into the neighboring stable region. It was shown that the response of the system with nonzero derivative control gain converges to zero faster than that with zero derivative control gain.

The analytical boundaries of the Hsu–Bhatt–Vyshnegradskii stability chart for the delayed closed-loop system with $\bar{P} = 0$ were derived, and the stability regions appear as triangles in the $\bar{K} - \bar{R}$ plane. Stability boundaries, however, do not in general remain as straight lines for the system with $\bar{P} \neq 0$ nor can they be investigated analytically. Hence, a numerical discretization method, the Chebyshev spectral continuous time approximation (CSCTA), has been implemented to obtain the stability boundaries for the case in which $\bar{P} \neq 0$. The MATLAB dde23 integrator has been applied to obtain the time histories of the controlled system, which have been in agreement with the stability charts. In control design, it is usually important to design the gains of the closed-loop dynamics for a specified performance such as critical damping. To achieve this, the criteria for a critically damped response were studied. The loci of the eigenvalues of the closed-loop linear delay differential equation along with numerical simulation indicate that the optimally critically damped parameter set obtained analytically achieves the best performance.

Unmodeled external torques due to effects such as atmospheric drag or bearing friction can cause steady-state attitude errors, which have been eliminated by adding a supplemental integral feedback term to the controller. This integral term has been sought through the inverse dynamics approach, in which similar steps to those given in the proof of the lemma have been followed. Then, the dynamics of the new closed-loop system have been studied. The advantage of including the additional integral term has been clarified by comparing the system response under the previous (actual) controller without the integral term to that under the recent (actual) controller with the integral term. There is no need for a priori knowledge of the unmodeled torque in this analysis.

Future work could consider the case where full 3×3 gain matrices P, K, and R occur in the closed-loop dynamics, which could be solved for via linear quadratic regulator theory, in combination with the CSCTA, for example. Although stability of the controlled response in this method would be guaranteed from the linear spectral stability, however, the derivation of the corresponding nonlinear control law would involve additional complexity and would differ from the actual control law for the case of the multiactuator control, as was illustrated in this paper. Additional related areas to pursue would be control gain selection by solving linear matrix inequality derived from the Lyapunov–Krasovskii theory and the implementation of a tracking control law.

Acknowledgments

Financial support from the National Science Foundation under Grant Nos. CMMI-0900289 and CMMI-1131646 is gratefully acknowledged.

References

[1] Hall, C., Tsiotras, P., and Shen, H., "Tracking Rigid Body Motion Using Thrusters and Momentum Wheels," *Journal of Astronautical Sciences*, Vol. 50, No. 3, 2002, pp. 311–323.

[2] Tsiotras, P., Shen, H., and Hall, C., "Satellite Attitude Control and Power Tracking with Energy/Momentum Wheels," *Journal of Guidance, Control, and Dynamics*, Vol. 24, No. 1, 2001, pp. 23–34. doi:10.2514/2.4705

[3] Schaub, H., and Junkins, J., *Analytical Mechanics of Space Systems*, AIAA, Reston, VA, 2009, pp. 406–408.

[4] Paielli, R., and Bach, R., "Attitude Control with Realization of Linear Error Dynamics," *Journal of Guidance, Control, and Dynamics*, Vol. 16, No. 1, 1993, pp. 182–189. doi:10.2514/3.11444

[5] Schaub, H., Akella, M. R., and Junkins, J. L., "Adaptive Control of Nonlinear Attitude Motions Realizing Linear Closed Loop Dynamics," *Journal of Guidance, Navigation, and Control*, Vol. 24, No. 1, 2001, pp. 95–100. doi:10.2514/2.4680

[6] Chunodkar, A., and Akella, M., "Attitude Stabilization with Unknown Bounded Delay in Feedback Control Implementation," *Journal of Guidance, Control, and Dynamics*, Vol. 34, No. 2, 2011, pp. 533–542. doi:10.2514/1.50352

[7] Ailon, A., Segev, R., and Arogeti, S., "A Simple Velocity-Free Controller for Attitude Regulation of a Spacecraft with Delayed Feedback," *IEEE Transactions on Automatic Control*, Vol. 49, No. 1, 2004, pp. 125–130. doi:10.1109/TAC.2003.821406

[8] Samiei, E., Nazari, M., Butcher, E., and Schaub, H., "Delayed Feedback Control of Rigid Body Attitude Using Neural Networks and Lyapunov-Krasovskii Functionals," *AAS/AIAA Spaceflight Mechanics Meeting*, AIAA Paper 0012-0168, Jan.–Feb. 2012.

[9] Insperger, T., and Stépán, G., *Semi-Discretization for Time-Delay Systems, Stability and Engineering Applications*, Springer–Verlag, New York, 2011, pp. 19–25.

[10] Stépán, G., *Retarded Dynamical Systems: Stability and Characteristic Functions*, Longman Scientific and Technical, Harlow, England, U.K., 1989, pp. 8–44.

[11] Butcher, E., and Bobrenkov, O., "On the Chebyshev Spectral Continuous Time Approximation for Constant and Periodic Delay Differential Equations," *Communications in Nonlinear Science and Numerical Simulation*, Vol. 16, No. 3, 2011, pp. 1541–1554. doi:10.1016/j.cnsns.2010.05.037

[12] Bobrenkov, O., Butcher, E., and Mann, B., "Application of the Liapunov-Floquet Transformation to Differential Equations with Time Delay and Periodic Coefficients," *Journal of Vibration and Control*, Vol. 19, No. 4, 2013, pp. 521–537. doi:10.1177/1077546311433914

[13] Bobrenkov, O., Nazari, M., and Butcher, E., "Response and Stability Analysis of Periodic Delayed Systems With Discontinuous Distributed Delay," *Journal of Computational and Nonlinear Dynamics*, Vol. 7, No. 3, 2012, Paper 031010. doi:10.1115/1.4005925